Journal of
Materials in Life Sciences

Vol. 4 No. 1 (2025)

Full Paper

Green Magnetic Adsorbent Functionalized with Humic Acid for Efficient Removal of Saxitoxin from Water

LaiZhi Bong[a], NyukTing Ng[a], Aemi Syazwani Abdul Keyon[a,b]*

[a]Department of Chemistry, Faculty of Science, Universiti Teknologi Malaysia, 81310 UTM Johor Bahru, Johor, Malaysia.
[b]Centre for Sustainable Nanomaterials (CsNano), Ibnu Sina Institute for Scientific and Industrial Research, Universiti Teknologi Malaysia, 81310 UTM Johor Bahru, Johor, Malaysia.

Article history
Received
21 April 2025
Revised
07 May 2025
Accepted
26 May 2025
Published online
31 May 2025

*Corresponding author
aemi@utm.my

Abstract

Water contamination by saxitoxin (STX), originating from harmful algal blooms intensified by anthropogenic eutrophication, poses a serious ecological and public health concern due to its potent neurotoxicity. This study developed a novel, eco-friendly magnetic humic acid-functionalized adsorbent (Fe_3O_4-HA) for STX removal from water. Fe_3O_4-HA was synthesized via co-precipitation, followed by humic acid (HA) functionalization. Successful synthesis was confirmed using Fourier-transform infrared spectroscopy, scanning electron microscopy with energy dispersive X-ray spectroscopy, and vibrating sample magnetometry, revealing the presence of key functional groups, heterogeneous morphology, elemental composition (C, O, Fe), and paramagnetic properties (23.385 emu/g). The point of zero charge (pH 2.5) indicated the surface neutrality threshold. Batch adsorption parameters: solution pH, adsorbent dosage, contact time, and STX concentration were optimized. Maximum STX removal (71.04%) occurred at natural solution pH (7.94) using 30 mg of adsorbent, within 8 min, at an initial STX concentration of 100 µg/L. Kinetic analyses demonstrated that the adsorption followed a pseudo-second-order model (R^2 = 0.9983), indicating chemisorption as the dominant mechanism. Multiple interactions were proposed, including electrostatic attraction, hydrogen bonding, and π-π interactions between negatively charged functional groups in HA and STX. An analytical eco-scale evaluation yielded a score of 81, classifying the synthesis as environmentally friendly. Comparison with existing methods confirmed that Fe_3O_4-HA offers superior adsorption efficiency, rapid action, and eco-sustainability. Thus, Fe_3O_4-HA represents a promising adsorbent for practical environmental remediation of STX-contaminated waters, warranting further studies for real-world scalability and applicability.

Keywords adsorption, magnetized adsorbent, humic acid, paralytic shellfish toxin, saxitoxin

1.0 INTRODUCTION

Human activities, such as urbanization and industrial wastewater discharge, elevate phosphorus and nitrogen levels in rivers and lakes, leading to water quality degradation (Le Moal *et al.*, 2019). This nutrient enrichment encourages the excessive growth of cyanobacteria, dinoflagellates, diatoms, and green algae, collectively known as harmful algal blooms (HABs). HABs produce saxitoxin (STX), a potent paralytic shellfish toxin (PST) that functions as a neurotoxin that poses significant threats to human and animal health while worsening the global water crisis (Zhang *et al.*, 2023). The occurrence of HABs has been rising globally, with significant events reported in North America, Europe, and Asia. In North America, recurring outbreaks in

the Gulf of Maine have led to large-scale paralytic shellfish poisoning (PSP) events, severely affecting the local shellfish industry and public health (Anderson *et al.*, 2019). Similarly, in Europe, blooms of Alexandrium species in the North Sea have caused widespread shellfish contamination, leading to commercial harvesting bans (Townhill *et al.*, 2018). In Malaysia, significant HAB occurrences in Sepanggar Bay, Sabah, between 2018 and 2019, predominantly involving Margalefidinium polykrikoides and Pyrodinium bahamense var. compressum, caused PSP, fish mortality, and seawater discoloration, impacting the local fisheries and public health (Lorons *et al.*, 2022). The rising frequency of HABs underscores the urgent need for effective monitoring and management strategies to mitigate their harmful effects on coastal waters worldwide.

Conventional methods for removing STX from water, such as chlorination, ozonation, and membrane filtration, present significant advantages and drawbacks (Kumar *et al.*, 2018). Chlorination can eliminate over 99.1% of STX, but it requires pH levels above 8, which is difficult to maintain in large-scale operations (Kumar *et al.*, 2018). Ozonation achieves 90-95% removal efficiency but generates harmful by-products and requires large amounts of oxidizing agents. Membrane filtration removes 90-100% of STX, but it is susceptible to membrane fouling over time, requiring regular cleaning and maintenance (Kulabhusan & Campbell, 2024). These challenges highlight the need for more sustainable and efficient STX removal methods. Given these limitations, adsorption presents as a promising alternative due to its versatility, wide applicability, and cost-effectiveness (Chambers *et al.*, 2024). Adsorption, widely studied for removing various contaminants, including organic compounds, heavy metals, and toxins (Pillai, 2020), allows targeted removal of specific contaminants by selecting appropriate adsorbents, facilitating efficient removal of STX even at low concentrations (Tran, 2023). Advances in nanomaterials and bio-based adsorbents have significantly enhanced adsorption capacity (q) and selectivity, improving the feasibility of this method (Tran, 2023).

Conventional non-magnetic adsorbents, though effective for contaminant removal, frequently suffer from poor reusability and difficult recycling, which can lead to secondary pollution (Ahmad Wani *et al.*, 2022). Recently, magnetite (Fe_3O_4)-based adsorbents have gained attention for their unique magnetic properties, versatility, ease of modification, and availability in various forms (Liu et al., 2023). Fe_3O_4 particles are easy to synthesize, cost-effective, and environmentally friendly (Liu et al., 2023). Most notably, their strong magnetic properties enable easy recovery after adsorption (Fu *et al.*, 2023). However, pristine Fe_3O_4 exhibits a relatively low q and tends to agglomerate in water, reducing its efficiency (Nguyen *et al.*, 2021). Kang *et al.* (2024) reported that pristine Fe_3O_4 removed only 56% of ciprofloxacin after 120 min, while Fe_3O_4 functionalized with sepiolite achieved 93% removal in just 60 min. To overcome these limitations, Fe_3O_4 particles are frequently modified with functional groups or other materials to enhance q and prevent agglomeration (Keshta *et al.*, 2024).

Humic acid (HA), abundant in natural sources such as soil, rocks, and animal waste (María de Lourdes *et al.*, 2022), contains abundant functional groups such as carboxyl, carbonyl, amino, phenyl and phenolic hydroxyl that act as effective adsorption sites for contaminant removal. Functionalizing Fe_3O_4 with HA also improves its dispersion properties by minimizing particle aggregation. This is due to the hydrophilic nature of HA, which creates a stabilizing layer around the nanoparticles, thereby minimizing van der Waals forces and steric hindrance (Pormazar *et al.*, 2020). Santosa *et al.* (2021) synthesized magnetic humic acid-functionalized adsorbent (Fe_3O_4-HA) for the reductive adsorption of Au(III) ion in aqueous solutions and reported an optimum q of 200 mg/g at pH 3.5 based on Langmuir isotherm model. Although Fe_3O_4-HA has been studied for heavy metals removal, its potential application for STX adsorption remains unexplored. In this study, a green Fe_3O_4-HA was synthesized through co-precipitation and surface modification techniques for the removal of STX from water.

2.0 EXPERIMENTAL

2.1 Materials

Goat dung was collected from residential areas in Kampung Kubang Jawi, Alor Janggus, 06250 Alor Setar, Kedah, Malaysia. Saxitoxin dihydrochloride (STX·2HCl) was obtained from the National Research Council of Canada. Sodium hydroxide pellets (NaOH) were acquired from QrëC (New Zealand). Hydrochloric acid (HCl, 37%) and hydrogen peroxide (H_2O_2, 30%) were sourced from Merck (Germany). Iron(II) sulfate heptahydrate ($FeSO_4·7H_2O$, AR/ACS Grade) was procured from HmbG Chemicals (Germany). Iron(III) chloride hexahydrate ($FeCl_3·6H2O$), sodium chloride (NaCl), glacial acetic acid (CH_3COOH, ≥99.0%) and Rhodamine 6G were all purchased from Sigma-Aldrich (USA). All chemicals were used as received, without further purification.

2.2 Apparatuses and instrumentations

Apparatuses used in this study included a sieve (Farmer, China), a blender (Cuisinart, USA), an analytical balance (Shimadzu, Japan), an oven (Hettich, Germany), a pH meter (Eutech, UK), a stirring hotplate (FAVORIT, Italy) and a vortex mixer (IKA, USA). For material characterization, instruments like Fourier-transform infrared spectroscopy (FTIR) (Shimadzu IR Tracer-100, Japan), scanning electron microscopy (SEM) (Hitachi TM3000, Japan), energy dispersive X-ray spectroscopy

(EDX) (Hitachi SwiftED 3000, Japan) and vibrating sample magnetometry (VSM) (LakeShore 7404, USA) were used. For STX detection, aqueous samples (300 µL of oxidized STX prepared in 50 µL-sized cuvettes) were studied by a fluorescence spectrophotometer (Agilent Eclipse, USA), operating with an excitation spectral bandwidth of 5 nm, an emission spectral bandwidth of 20 nm, an excitation wavelength of 334 nm and an emission wavelength of 548 nm.

2.3 Extraction of humic acid

Goat dung was collected, sun-dried, ground and sieved to a 200-mesh size. Subsequently, 100 g of the powdered dung was added to 1 L of 0.1 mol/L NaOH solution. The mixture was gently stirred for 24 h (Santosa *et al.*, 2021). The supernatant was separated via centrifugation at 2000 rpm for 20 min. The supernatant was then acidified to approximately pH 1 by gradually adding 0.01 mol/L HCl, causing the precipitation of HA. The precipitate was then collected via centrifugation at 2000 rpm for 20 min and dried at 50°C overnight to obtain a crude HA.

2.4 Synthesis of magnetic humic acid-functionalized adsorbent

Fe_3O_4 was synthesized via co-precipitation. Simultaneously, the surface of Fe_3O_4 was modified by coating it with HA (Shen *et al.*, 2023). During co-precipitation, 1 mol/L NaOH was employed as the precipitating agent. A mixture of 2.78 g of $FeSO_4 \cdot 7H_2O$ (0.01 mol) and 5.41 g of $FeCl_3 \cdot 6H_2O$ (0.02 mol) was dissolved in 100 mL of distilled water and stirred at 90°C. Then, 1 g of HA was added to the stirring mixture (Santosa et al., 2021). At this stage, NaOH was added dropwise to the mixture until the pH reached 11 (Ba-Abbad *et al.*, 2022)After 30 min, vigorous stirring was stopped, and the mixture was allowed to settle at room temperature. The resulting precipitate was filtered through a 0.45 µm membrane and rinsed with distilled water until a neutral pH was achieved. Finally, the Fe3O4-HA was dried in an oven at 75°C for 24 h. The adsorbent was stored in a desiccator before use.

2.5 Preliminary studies

Preliminary studies were conducted with 1 mg/L Rhodamine 6G to evaluate the q of Fe_3O_4-HA. 20 mg of Fe_3O_4-HA was added to 10 mL of 1 mg/L Rhodamine 6G solution and vortexed for 10 min. At specific time intervals (1, 2, 4, 6, 8 and 10 min), the color intensity of the solution was observed. After 10 min, Fe_3O_4-HA was separated from the solution using a magnet. Finally, the fluorescence intensity of Rhodamine 6G was measured using a fluorescence spectrophotometer, with an excitation wavelength of 525 nm and an emission wavelength of 548 nm.

2.6 Optimization of the adsorption process

2.6.1 Effect of solution pH

A series of 2 mL STX (50 µg/L) solutions was prepared, with solution pH levels adjusted to 4, 6, 8 and one left at its natural pH of 7.94. 10 mg of Fe_3O_4-HA was added to each solution, and the mixtures were stirred for 10 min. Then, Fe_3O_4-HA was separated from the solutions using an external magnet. The STX solutions were collected and subjected to peroxide oxidation before analysis using a fluorescence spectrophotometer.

2.6.2 Effect of solution adsorbent dosage

A series of 2 mL STX (50 µg/L) solutions was prepared without adjusting their pH to retain a natural pH of 7.94. Fe_3O_4-HA, in masses of 5, 10, 30, 50 and 70 mg, was added to each solution and stirred for 10 min. Fe_3O_4-HA was then separated from the solutions using an external magnet. Finally, the STX solutions were collected and subjected to peroxide oxidation before analysis using a fluorescence spectrophotometer.

2.6.3 Effect of contact time

30 mg of Fe_3O_4-HA was added to 2 mL STX solutions (50 µg/L) at their natural solution pH (7.94). These mixtures were stirred at varying contact times, 1, 2, 4, 6, 8 and 10 min. Fe_3O_4-HA was then separated from the solutions using an external magnet. The resulting STX solutions were collected and subjected to peroxide oxidation before analysis using a fluorescence spectrophotometer. The experimental data obtained from this parameter were utilized to evaluate the adsorption mechanism with two kinetic models: PFO and PSO.

2.6.4 Effect of adsorbate concentration

30 mg of Fe_3O_4-HA was added to a series of 2 mL STX solutions at varying initial concentrations of 25, 50, 75 and 100 µg/L, at a natural solution pH of 7.94. The mixtures were stirred for 8 min, after which the Fe_3O_4-HA was separated using an external magnet. Lastly, the resultant STX solutions were collected, subjected to peroxide oxidation, and analyzed using a fluorescence spectrophotometer.

2.7 Peroxide oxidation for derivatization of STX

The peroxide oxidation method was modified from AOAC 2005.06 and adapted to enhance STX fluorescence before fluorescence spectroscopic analysis. 25 µL of 10% H_2O_2 solution and 250 µL of 0.4 M NaOH solution were added to a centrifuge tube and mixed under vortexing for 30 s. Subsequently, 100 µL of STX samples (post-adsorption) were added to the mixture and vortexed again for 3 min at room temperature. Lastly, 20 µL of glacial CH3COOH was added to the resulting mixture and vortexed for 30 s to terminate the oxidation process.

2.8 Kinetic studies

The PFO model assumes the adsorption rate is proportional to the number of unoccupied sites. This model is typically used in the initial stages of adsorption, when the adsorbate concentration significantly exceeds that of the adsorbent, resulting in a linear relationship between the adsorption rate and the adsorbate concentration (Revellame *et al.*, 2020). The PFO equation is given by:

$$\ln ln\,(q_e - q_t) = \ln ln\, q_e - \frac{k_1}{2.303} t \#(1)$$

where q_e and q_t represent the amount of solute adsorbed per unit mass of sorbent (mg/g) at time t and at equilibrium, respectively. k_1 represents the rate constant for PFO adsorption (min^{-1}). The plot of $\ln(q_e - q_t)$ versus t yields a slope equal to $\ln q_e$ and an intercept equal to $k_1/2.303$.

The PSO model describes an adsorption process where the driving force is related to the fraction of accessible adsorption sites. In this model, the adsorption rate depends on the square of the number of unoccupied sites. This model suggests that chemisorption, which involves valence forces and electron sharing or exchange between the adsorbent and adsorbate, controls the rate-limiting step (Revellame *et al.*, 2020). The PSO equation is given by:

$$\frac{t}{q_t} = \frac{1}{k_2 q_e^{\,2}} + \left(\frac{1}{q_e}\right) t \#(2)$$

where k_2 (g/mg min) is the rate constant for PSO adsorption.

3.0 RESULTS AND DISCUSSION

3.1 Characterization of Fe_3O_4-HA

FTIR analysis was performed to analyze the chemical composition and identify the functional groups in HA, Fe_3O_4, and Fe_3O_4-HA. Figure 1(a) presents the FTIR spectra of HA, Fe_3O_4 and Fe_3O_4-HA. HA exhibits absorption bands at 3420, 2920, 1652 and 1547 cm^{-1}, corresponding to O-H stretching in phenolic groups, C-H stretching in aliphatic methylene groups, O-H bending in hydroxyl groups, and N-H in-plane bending from amides, respectively. The absorption band at 1228 cm^{-1} is attributed to C=O stretching in carboxyl groups and C-O stretching in carboxyl groups, aryl esters and phenols. The band at 1075 cm^{-1} is likely due to C-O stretching from polysaccharides (Fernández-Delgado *et al.*, 2023). Fe_3O_4 exhibits characteristic absorption bands at 3368, 1624, and 587 cm^{-1}, corresponding to O-H stretching (due to adsorbed water) O-H bending, and Fe-O stretching, respectively. After surface modification of Fe_3O_4 with HA, the intensities of O-H stretching and bending absorption bands increased, with new peaks emerging at 1547, 1230 and 1106 cm^{-1}. These changes confirm the successful interaction between Fe atoms in Fe3O4 and functional groups in HA (Santosa *et al.*, 2021).

Understanding an adsorbent's surface charge allows for the effective manipulation of adsorbent-adsorbate interactions (Ng *et al.*, 2023). Figure 1(b) illustrates the point of zero charge analysis, pH_{PZC} of Fe_3O_4-HA. The pH_{PZC} of Fe_3O_4-HA was determined to be pH 2.5, based on the intersection point of the graph on the x-axis. At solution pH levels below 2.5, the surface undergoes protonation, resulting in the accumulation of hydrogen ions and a positive surface charge. Conversely, at pH levels above 2.5, the adsorbent's surface releases hydroxide ions, corresponding to a negative surface charge. This pH-dependent behavior elucidates the adsorption mechanism of STX with Fe_3O_4-HA. By considering the pH of the sample at 7.94 during the removal process, STX predominantly exists in cationic form, with a small fraction in neutral form

(Shi *et al.*, 2012). Electrostatic interactions are expected to dominate the cationic fraction of STX at this pH, while non-electrostatic interactions (e.g. London Dispersion Forces) are likely influential for the neutral fraction (Shi *et al.*, 2012).

SEM provides valuable information on morphological changes following adsorbent modification. Alterations in surface heterogeneity or surface area can influence the mass transfer of analytes to Fe_3O_4-HA (Nazari *et al.*, 2022). Figure 1(c) presents the SEM images of HA, Fe_3O_4 and Fe_3O_4-HA. HA exhibits a flaky surface, whereas agglomeration is observed on the Fe_3O_4 surface. The SEM image of Fe_3O_4-HA reveals a heterogeneous surface morphology with particles of varying sizes. The particles appear agglomerated, suggesting a non-uniform coating of HA on the Fe_3O_4 particles. Further evidence is provided by the EDX results in Table 1, which show changes in the weight percentages of elements in Fe_3O_4-HA compared to HA and Fe_3O_4. The presence of carbon (20.7%) in Fe_3O_4-HA confirms the attachment of HA on the Fe_3O_4 surface.

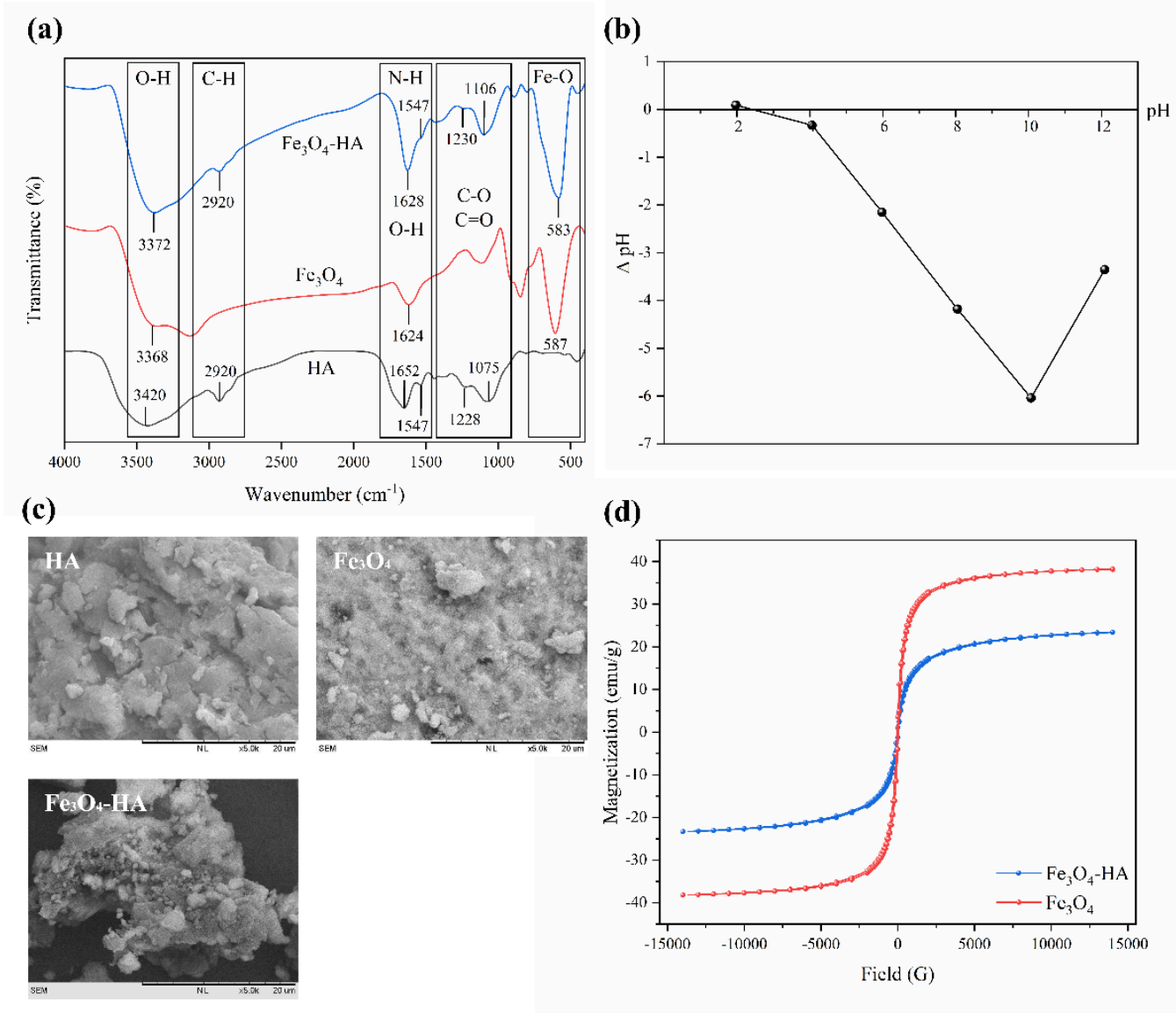

Figure 1 (a) FTIR spectra of HA, Fe_3O_4, Fe_3O_4-HA), (b) Surface charge analysis of Fe_3O_4-HA, (c) SEM images of HA, Fe_3O_4, Fe_3O_4-HA, and (d) Magnetization curve of Fe_3O_4 and Fe_3O_4-HA

Table 1 EDX results of HA, Fe_3O_4, and Fe_3O_4-HA

	Weight Percentage (%)		
Element	**HA**	**Fe_3O_4**	**Fe_3O_4-HA**
C	49.7	-	20.7
O	50.3	20.7	25.6
Fe	-	79.3	53.7

Table 2 Magnetic parameters of Fe_3O_4 and Fe_3O_4-HA

Material	M_s (emu/g)	H_c (G)	M_r (emu/g)	M_r/M_s
Fe_3O_4	38.231	42.893	3.8152	9.9793×10^{-3}
Fe_3O_4-HA	23.285	30.993	1.1356	4.8561×10^{-3}

Figure 1(d) shows the hysteresis curves obtained by VSM for Fe_3O_4 and Fe_3O_4-HA, with magnetic parameters such as saturation magnetization (M_s), retentivity (M_r) and coercivity (H_c) summarized in Table 2. The magnetization of both Fe_3O_4 and Fe_3O_4-HA increases with the applied magnetic field until reaching saturation. Both materials are paramagnetic, with squareness values (M_r/M_s) close to zero. The low M_r values indicate that both materials can be easily separated using an external magnet (Abbas *et al.*, 2024). The incorporation of HA onto Fe_3O_4 results in lower values of M_s, H_c and M_r. This suggests that functionalizing Fe_3O_4 with non-magnetic HA negatively affects its magnetic properties, likely due to the formation of Fe-O-C bonds (Abbas *et al.*, 2024).

3.2 Preliminary study on Rhodamine 6G removal

In this preliminary study, Rhodamine 6G was used as a model compound for STX removal. Since both STX and Rhodamine 6G contain amine groups, interactions of these compounds with the adsorbent, Fe_3O_4-HA might be similar. This makes Rhodamine 6G a suitable stand-in for STX in these preliminary studies. Based on Figures 2(a) and (b), a decrease in both colour and fluorescence intensities for Rhodamine 6G adsorption indicates its successful adsorption onto Fe_3O_4-HA. This suggests the adsorbent Fe_3O_4-HA has tremendous potential for STX, as evidenced by the preliminary study in which Fe_3O_4-HA eliminated Rhodamine 6G by about 95.2%.

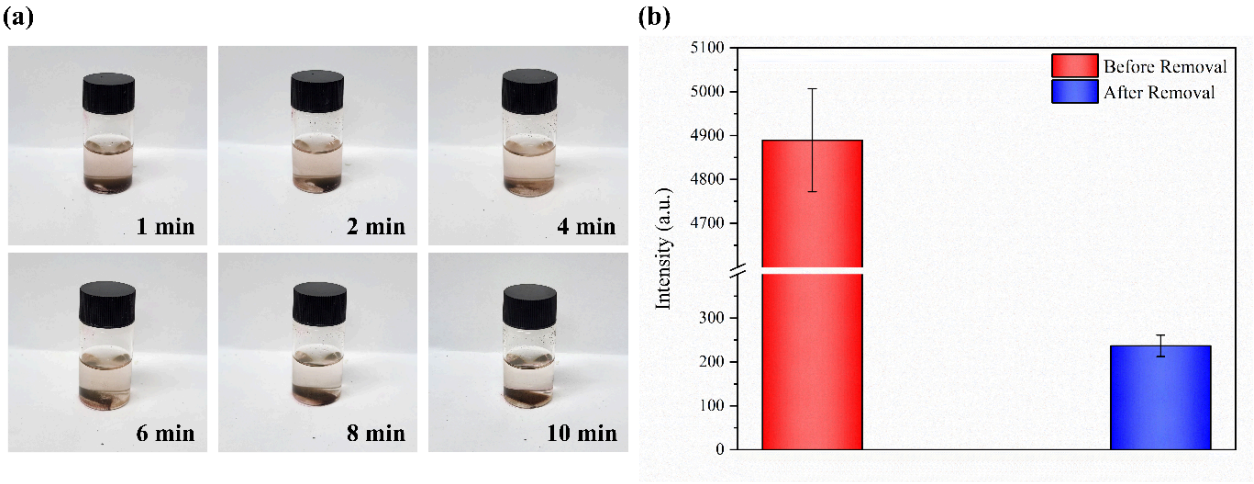

Figure 2 (a) Color intensity of Rhodamine 6G solution at different time intervals of adsorption time, (b) Fluorescence intensity of Rhodamine 6G before and after removal.

3.3 Optimization of the adsorption process

In this work, adjusting the solution pH could negatively impact STX removal. This is due to the optimum pH for STX derivatization was 12.2 (Gago-Martínez *et al.*, 2001). Thus, any changes in the initial solution pH during the removal process may shift the pH away from the optimum derivatization level. Such deviation can result in a complete failure of derivatized STX detection by fluorescent spectroscopy. Therefore, successful STX removal was achieved at a natural solution pH of 7.94. This might be attributed to the electrostatic and non-electrostatic interactions between STX and Fe_3O_4-HA, as Fe3O4-HA adsorbent exhibited a net negative surface charge at this pH (as supported by its surface charge analysis, where its pH_{PZC} is 2.5). Thus, electrostatic interactions are expected to dominate as a major cationic fraction of STX exists at this pH, while non-electrostatic interactions (e.g., London Dispersion Forces) likely influence the minor neutral fractions of STX (Shi *et al.*, 2012).

The effect of Fe_3O_4-HA dosage on STX adsorption was investigated across a range of doses (5, 10, 30, 50 and 70 mg), as illustrated in Figure 3(a). Increasing the dosage of Fe_3O_4-HA led to an increment in STX removal efficiency, from 38.8% to 63.7%. This increment can be attributed to a greater number of active sites for STX adsorption as the Fe_3O_4-HA dosage increases (Rápó & Tonk, 2021). Consequently, this results in a higher percentage of STX removal. However, when the adsorbent dosage exceeded 30 mg, the STX removal percentage decreased. This decrement may be attributed to the agglomeration of Fe_3O_4-HA particles (Popa *et al.*, 2021). A high adsorbent-to-liquid ratio can cause adsorbent agglomeration, leading to a reduction in the effective surface area of Fe_3O_4-HA (Amirmahani *et al.*, 2020).

The effect of contact time on STX adsorption was examined over a time range of 1, 2, 4, 6, 8 and 10 min. As illustrated in Figure 3(b), the STX removal percentage increased from 37.9% to 62.5% with an increasing contact time, reaching equilibrium at 8 min. This indicates that the adsorbent becomes saturated with the adsorbate at equilibrium (Pini *et al.*, 2022).

The initial adsorbate concentration is a critical factor affecting the adsorption efficiency of an adsorbent. Figure 3(c) illustrates the effect of initial adsorbate concentration on the removal efficiency of STX. A maximum removal efficiency of 71.0% was observed at an initial STX concentration of 100 µg/L. At low initial concentrations, there may not be enough STX molecules to occupy all available adsorption sites on the adsorbent. In contrast, when the initial STX concentration increases, more adsorption sites are occupied, thereby increasing the removal efficiency. This is because the higher initial STX concentrations could generate a stronger driving force for STX to migrate from the solution to the adsorbent surface (Svobodová *et al.*, 2024).

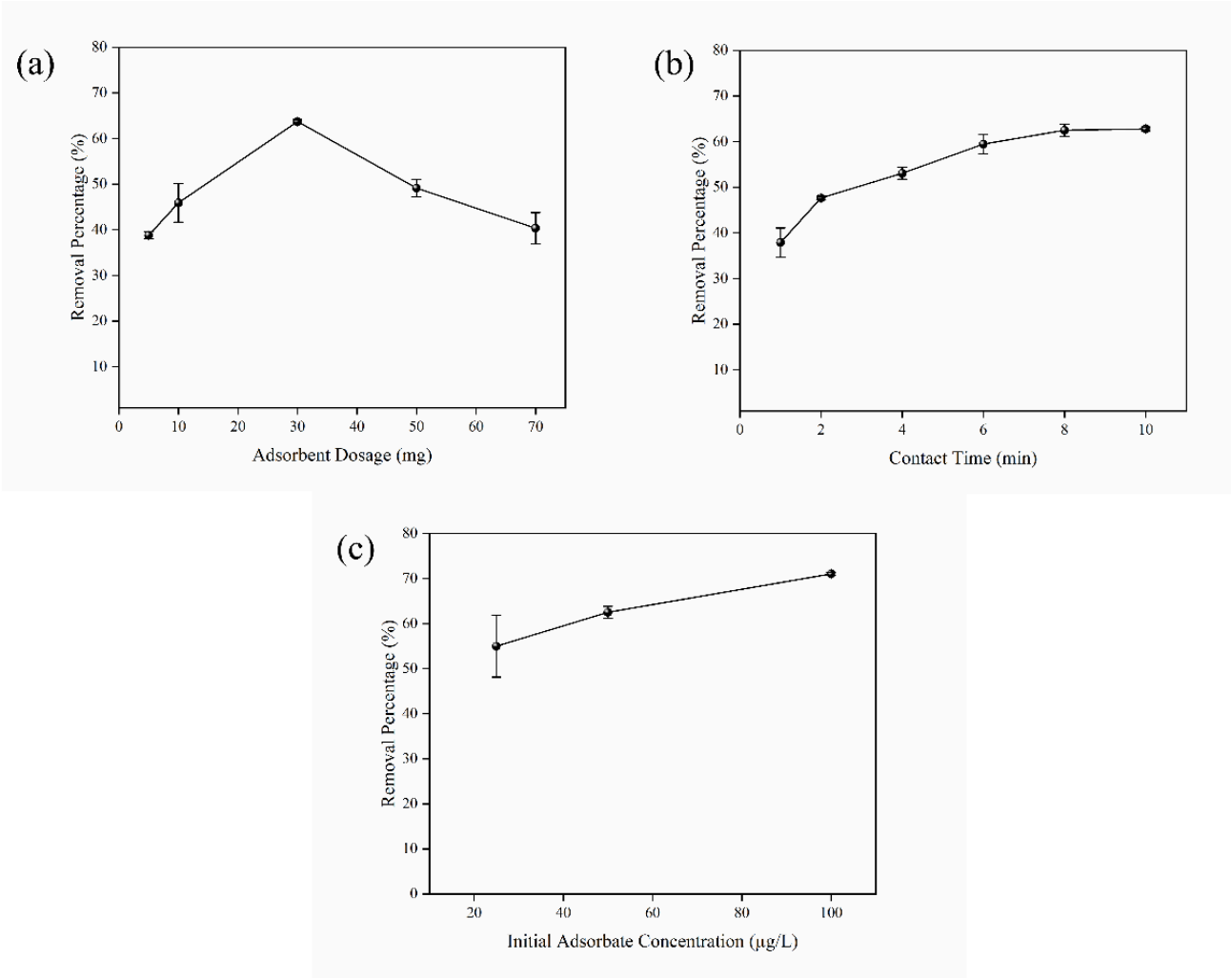

Figure 3 (a) Effect of adsorbent dosage on STX removal (Other removal parameters: solution pH = 7.94; contact time = 10 min; initial adsorbate concentration = 50 µg/L); (b) Effect of contact time on STX removal (Other removal parameters: solution pH = 7.94; adsorbent dosage = 30 mg; initial adsorbate concentration = 50 µg/L); (c) Effect of initial adsorbate concentration on STX removal (Other removal parameters: solution pH = 7.94; adsorbent dosage = 30 mg; contact time = 8 min).

3.3 Kinetic studies

The adsorption kinetics of STX onto Fe_3O_4-HA, as shown in Figure 4, exhibited rapid initial uptake, followed by a gradual increase and eventual plateau after 8 min. The estimated kinetic parameters in Table 3 indicate that the R^2 value of the PSO kinetic model is 0.9983, which is higher than that of the PFO model (0.7803). This indicates that the PSO model describes STX adsorption better compared to the PFO model. As reported in the literature, the PFO kinetic model is associated with physisorption, while the PSO model corresponds to chemisorption processes (Sayed *et al.*, 2024). Consequently, the kinetic data suggest that STX adsorption onto Fe_3O_4-HA occurs primarily through chemisorption. Additionally, the PSO model's calculated equilibrium capacity for STX (q_e = 0.002215 mg/g) was closer to the experimental q_e value (0.0022 mg/g) than the PFO model's value (q_e = 0.0007463 mg/g).

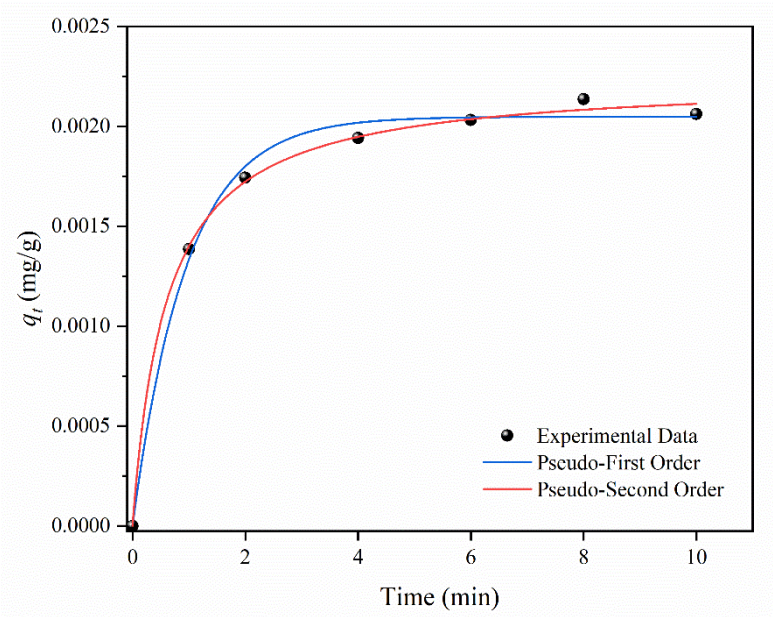

Figure 4 Kinetic studies of saxitoxin (STX) removal (Removal parameters: solution pH = 7.94; adsorbent dosage = 30 mg; contact time = 8 min; initial adsorbate concentration = 50 µg/L).

Table 3 Kinetic parameters of STX adsorption onto Fe_3O_4-HA

Model	Parameter	
Pseudo-First-Order	q_e (mg/g)	0.0007463
	k_1 (min^{-1})	0.23
	R^2	0.7803
Pseudo-Second-Order	q_e (mg/g)	0.002215
	k_2 (g mg^{-1} min^{-1})	827.4
	R^2	0.9983
Experimental Data	q_e (mg/g)	0.0022

3.4 Proposed interactions between Fe_3O_4-HA and STX

Several interactions between Fe_3O_4-HA and STX, including electrostatic interactions, hydrogen bonding and π-π interactions are proposed and illustrated in Figure 5. The presence of carboxyl, phenolic, and hydroxyl groups in the negatively charged HA might facilitate strong electrostatic interactions with the positively charged sites on STX molecules. These functional groups also could facilitate hydrogen bond formation with STX molecules, further enhancing adsorption. Furthermore, the aromatic structures in HA might participate in the π-π interactions with the aromatic rings of STX. These synergistic interactions enhance the q and stability of the Fe_3O_4-HA, making it a promising candidate for effective STX removal from aqueous solutions.

3.5 Analytical eco-scale evaluation

Table 4 presents an analytical eco-scale calculation for Fe3O4-HA synthesis. After careful calculation, a total score of 81 was obtained, indicating that the method qualifies as an excellent green analytical procedure. The primary contributors to the penalty points (PP) are the reagents, particularly HCl and FeCl3·6H2O, both of which are classified as high-hazard substances. The process shows very low energy consumption, contributing only 1 penalty point and highlighting its energy efficiency. However, the waste generated incurs an additional 5 PP. Implementing strategies to minimize or recycle this waste could significantly enhance the eco-scale score.

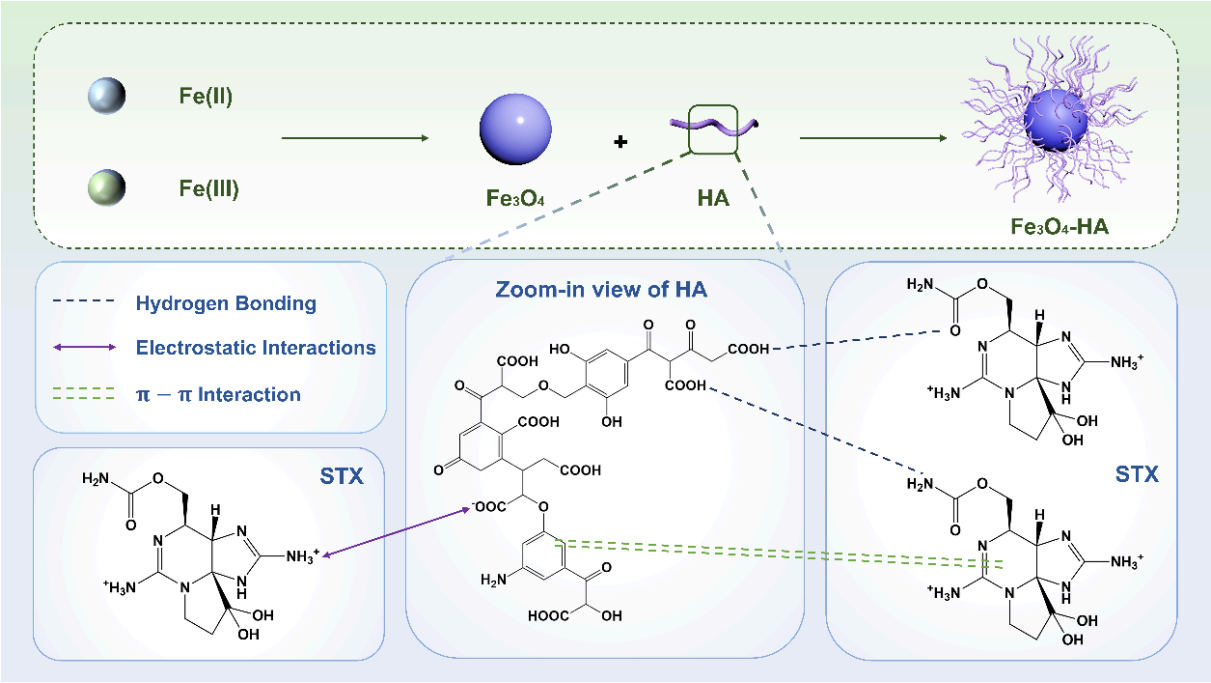

Figure 5 Proposed interaction between Fe_3O_4-HA and STX

Table 4 Analytical eco-scale calculation of Fe_3O_4-HA synthesis and adsorption process.

	Parameters			
Reagent	**Amount (PP)**	**Number of Pictogram (PP)**	**Signal Word (PP)**	**Calculated PP**
Goat dung	<10 g (1)	0 (0)	None (0)	1×0×0 = 0
Sodium hydroxide	<10 mL (1)	1 (1)	Danger (2)	1×1×2 = 2
Hydrochloric acid	<10 mL (1)	2 (2)	Danger (2)	1×2×2 = 4
Hydrogen peroxide	<10 mL (1)	1 (1)	Danger (2)	1×1×2 = 2
Iron(II) sulfate heptahydrate	<10 g (1)	1 (1)	Warning (1)	1×1×1 = 1
Iron(III) chloride hexahydrate	<10 g (1)	2 (2)	Danger (2)	1×2×2 = 4
Water	>100 mL (4)	0 (0)	None (0)	4×0×0 = 0
Total PP for reagent used				**13**
Instrument	**Energy used per sample (kWh) (PP)**			**Calculated PP**
Centrifuge	≤1.5 (1)			1
Stirring hotplate	≤0.1 (0)			0
Oven	≤1.0 (0)			0
Vortex mixer	≤0.1 (0)			0
Total PP for energy used				**1**
Other				
Waste	>10 mL			5
Occupational hazard	Hermitization in analytical process (0)			0
Total PP for other				**5**
Total PP				13+1+5 = 19
Analytical Eco-scale total score				100−27 = **81 (Excellent)**

* kWh, kilowatt per hour; PP, penalty point(s).

3.6 Comparison with other reported methods

Table 5 shows a comparison of Fe_3O_4-HA with other reported adsorbents such as oyster shells, chitin, granular activated carbon (GAC), alginate gel, carrageenan gels and covalent organic polymers for STX removal from water. Melegari and Matias (2012) found that oyster shells and chitin-based materials were able to remove over 50% of STX within 18 h. However, their adsorption performance decreased with prolonged contact time, likely due to the adsorption site saturation, indicating that ion exchange was the main mechanism involved. The study employed four coconut shell granular activated carbons (GACs), designated as C1, C2, C3, and C4, with the experimental temperature controlled at 28°C. Under pH 7.0, electrostatic

repulsion was determined to be the dominant mechanism, accounting for the low adsorption capacities. Moreover, the presence of dissolved organic matter (DOM) hindered the adsorption of STX via two mechanisms: (a) micropore blockage by high molecular weight DOM and (b) preferential adsorption of DOM, which, due to its negative charge, was electrostatically attracted to the positively charged adsorbent surfaces. Olano *et al.* (2020) evaluated the adsorption performance of algal polysaccharide gels, including alginate, refined carrageenan (RC), and semi-refined carrageenan (SRC), for the removal of STX from deionized water. Experiments were performed at pH 7.0 and controlled temperatures of 25°C and 37°C. The maximum removal efficiencies for STX were 1.03, 1.26, and 1.04 µg/g, respectively. Alginate exhibited a sorptive capacity comparable to carrageenan and displayed ion exchange properties. The carboxylic acid groups of alginates formed electrostatic interactions with the cationic amine groups of STX. In contrast, the adsorption of STX on carrageenan was attributed to electrostatic interactions between the negatively charged sulfate groups of carrageenan and the positively charged amine groups of STX, as well as hydrogen bonding and complexation. Wang *et al.* (2023) synthesized a carboxyl-functionalized COP (TpPa-COOH), which exhibited effective adsorption of STX, achieving a maximum q of 5.69 mg/g. Furthermore, TpPa-COOH showed excellent reusability, underscoring its potential as a promising material for the removal of STX from aquatic environments.

Table 5 Comparison of the adsorption parameters of Fe_3O_4-HA with other reported adsorbents for STX removal from water

Adsorbent	Temperature (°C)	Solution pH	Adsorbent Dosage (g/L)	Equilibrium time (min)	q_e (mg/g)	Kinetic model	References
Fe_3O_4-HA	Room Temperature	7.94	15.0	8	0.00222	PSO	This study
Chitin	25	5.00	20.0	-	0.00327	PSO	Melegari and Matias (2012)
	25	7.00	20.0	2880	0.00500	PSO	
Oyster shell	25	5.00	20.0	-	0.00370	PSO	
	25	7.00	20.0	2880	0.00400	PSO	
CS GAC C1	28	7.00	0.3	1320	0.143	PSO	Silva *et al.* (2015)
CS GAC C2	28	7.00	0.3	1320	0.203	PSO	
CS GAC C3	28	7.00	0.3	900	0.252	PSO	
CS GAC C4	28	7.00	0.3	2100	0.239	PSO	
Alginate gel	25	7.00	-	60	0.00047	PFO	Olano *et al.* (2020)
	37	7.00	-	60	0.00026	PFO	
RC gel	25	7.00	-	60	0.00067	PFO	
	37	7.00	-	60	0.00027	PFO & PSO	
SRC gel	25	7.00	-	60	0.00048	PFO	
	37	7.00	-	60	0.00036	PFO & PSO	
TpPa-COOH	19	6.00-7.00	1.0	60	1.82	PFO & PSO	Wang *et al.* (2023)

*CS, coconut shell; Fe_3O_4-HA, magnetic humic acid-functionalized adsorbent; GAC, granular activated carbon; RC, refined carrageenan; SRC, semi-refined carrageenan; TpPa-COOH, carboxyl-functionalized COP

4.0 CONCLUSION

In this study, Fe_3O_4-HA was developed and characterized for its effectiveness in removing STX from aqueous solutions. The optimal conditions for maximum adsorption (71.0%) were identified, occurring at a natural solution pH of 7.94, an adsorbent dosage of 30 mg, and a contact time of 8 min with an initial adsorbate concentration of 100 µg/L. The adsorption kinetics were best described by a PSO model, indicating that chemisorption is the dominant mechanism, supported by a high correlation coefficient (R^2 = 0.9983). The equilibrium adsorption capacity (q_e = 0.002215 mg/g) closely matched the experimental value (q_e = 0.0022 mg/g), confirming the reliability of the developed adsorbent. In conclusion, these findings demonstrate that Fe_3O_4-HA is a promising material for the effective removal of STX from water, offering a robust solution for water purification applications. Future work could explore the scalability of this adsorbent and evaluate its performance in real-world water treatment scenarios.

Acknowledgment

The authors would like to thank Malaysia Ministry of Higher Education (MOHE) for funding this research through Fundamental Research Grant Scheme (registration number FRGS/1/2022/STG04/UTM/02/1, reference number: PY/2022/03336, cost center number: R.J130000.7854.5F528). The authors also thanked Kurita Asia Research Grant (grant number: 23Pmy005) provided by Kurita Water and Environment Foundation (KWEF).

References

Abbas, Z. M. A., Shatti, W. A., Mohammad, A. M., & Khodair, Z. T. (2024). Magnetic iron oxide: Preparation and characterization for antibacterial activity applications. *Journal of Sol-Gel Science and Technology, 109*(2), 534–542. https://doi.org/10.1007/s10971-023-06300-w

Ahmad Wani, A., Shahadat, M., Wazed Ali, S., Ziauddin Ahammad, S., & Kashif Uddin, M. (2022). Recent advances and future perspectives of polymer-based magnetic nanomaterials for detection and removal of radionuclides: A review. *Journal of Molecular Liquids, 365*, 119976. https://doi.org/10.1016/j.molliq.2022.119976

Amirmahani, N., Mahdizadeh, H., Malakootian, M., Pardakhty, A., & Mahmoodi, N. O. (2020). Evaluating nanoparticles decorated on Fe_3O_4@SiO_2-Schiff base (Fe_3O_4@SiO_2-APTMS-HBA) in adsorption of ciprofloxacin from aqueous environments. *Journal of Inorganic and Organometallic Polymers and Materials, 30*(9), 3540–3551. https://doi.org/10.1007/s10904-020-01499-5

Anderson, C. R., Berdalet, E., Kudela, R. M., Cusack, C. K., Silke, J., O'Rourke, E., Dugan, D., McCammon, M., Newton, J. A., Moore, S. K., Paige, K., Ruberg, S., Morrison, J. R., Kirkpatrick, B., Hubbard, K., & Morell, J. (2019). Scaling up from regional case studies to a global harmful algal bloom observing system [Review]. *Frontiers in Marine Science, 6*, 250. https://doi.org/10.3389/fmars.2019.00250

Ba-Abbad, M. M., Benamour, A., Ewis, D., Mohammad, A. W., & Mahmoudi, E. (2022). Synthesis of Fe_3O_4 nanoparticles with different shapes through a co-precipitation method and their application. *JOM, 74*(9), 3531–3539. https://doi.org/10.1007/s11837-022-05380-3

Chambers, C., Grimes, S., Fire, S., & Reza, M. T. (2024). Influence of biochar on the removal of Microcystin-LR and saxitoxin from aqueous solutions. *Scientific Reports, 14*(1), 11058. https://doi.org/10.1038/s41598-024-61802-z

Fernández-Delgado, M., López-Linares, J. C., Lucas, S., García-Cubero, M. T., & Coca, M. (2023). Efficient recovery and characterization of humic acids from municipal and manure composts: A comparative study. *Waste Management, 172*, 245–255. https://doi.org/10.1016/j.wasman.2023.10.025

Fu, X., Sarker, S., Ma, W., Zhao, W., Rong, Y., & Liu, Q. (2023). Novel phenylalanine-modified magnetic ferroferric oxide nanoparticles for ciprofloxacin removal from aqueous solution. *Journal of Colloid and Interface Science, 632*, 345–356. https://doi.org/10.1016/j.jcis.2022.11.067

Gago-Martínez, A., Moscoso, S. A., Leão Martins, J. M., Rodriguez Vázquez, J.-A., Niedzwiadek, B., & Lawrence, J. F. (2001). Effect of pH on the oxidation of paralytic shellfish poisoning toxins for analysis by liquid chromatography. *Journal of Chromatography A, 905*(1), 351–357. https://doi.org/10.1016/S0021-9673(00)00963-8

Kang, S., Yi, B., Nie, X., Wan, Q., & Yang, H. (2024). Boosting adsorption of ciprofloxacin on Fe_3O_4 nanoparticles modified sepiolite composite synthesized via a vacuum-filtration assisted coprecipitation strategy. *Journal of Water Process Engineering, 66*, 106038. https://doi.org/10.1016/j.jwpe.2024.106038

Keshta, B. E., Gemeay, A. H., Sinha, D. K., Elsharkawy, S., Hassan, F., Rai, N., & Arora, C. (2024). State of the art on the magnetic iron oxide nanoparticles: Synthesis, functionalization, and applications in wastewater treatment. *Results in Chemistry, 7*, 101388. https://doi.org/10.1016/j.rechem.2024.101388

Kulabhusan, P. K., & Campbell, K. (2024). Physico-chemical treatments for the removal of cyanotoxins from drinking water: Current challenges and future trends. *Science of the Total Environment, 917*, 170078. https://doi.org/10.1016/j.scitotenv.2024.170078

Kumar, P., Hegde, K., Brar, S. K., Cledon, M., & Pour, A. K. (2018). Physico-chemical treatment for the degradation of cyanotoxins with emphasis on drinking water treatment—How far have we come? *Journal of Environmental Chemical Engineering, 6*(4), 5369–5388. https://doi.org/10.1016/j.jece.2018.08.032

Le Moal, M., Gascuel-Odoux, C., Ménesguen, A., Souchon, Y., Étrillard, C., Levain, A., ... & Pinay, G. (2019). Eutrophication: A new wine in an old bottle? *Science of the Total Environment, 651*, 1–11. https://doi.org/10.1016/j.scitotenv.2018.09.139

Lorons, D., Jafar-Sidik, M., Ali, N., Mohamad-Azaini, F., Rodrigues, K. F., & Chin, G. J. W. L. (2022). The variation of environmental profiles during harmful algal bloom in Sepanggar Bay, Sabah, Malaysia. *Journal of Oceanography, 78*(2), 121–132. https://doi.org/10.1007/s10872-022-00634-9

María de Lourdes, A., Sergio, G.-R., & Guillermo, T.-I. (2022). Mechanisms of action of humic substances as growth promoters in animals. In M. Abdelhadi (Ed.), *Humus and Humic Substances* (Ch. 2). IntechOpen. https://doi.org/10.5772/intechopen.105956

Melegari, S. P., & Matias, W. G. (2012). Preliminary assessment of the performance of oyster shells and chitin materials as adsorbents in the removal of saxitoxin in aqueous solutions. *Chemistry Central Journal, 6*(1), Article 86. https://doi.org/10.1186/1752-153X-6-86

Nazari, M. T., Schnorr, C., Rigueto, C. V. T., Alessandretti, I., Melara, F., da Silva, N. F., Crestani, L., Ferrari, V., Vieillard, J., Dotto, G. L., Silva, L. F. O., & Piccin, J. S. (2022). A review of the main methods for composite adsorbents

characterization. *Environmental Science and Pollution Research, 29*(59), 88488–88506. https://doi.org/10.1007/s11356-022-23883-z

Ng, N., Abdul Keyon, A. S., Wan Ibrahim, W. A., Sanagi, M. M., Sutirman, Z. A., & Mohd Marsin, F. (2023). Amino-functionalised chrysin as adsorbent in dispersive micro-solid phase extraction of selected heavy metal ions from stingless bee honey. *Journal of Food Composition and Analysis, 123*, 105561. https://doi.org/10.1016/j.jfca.2023.105561

Nguyen, M. D., Tran, H.-V., Xu, S., & Lee, T. R. (2021). Fe_3O_4 nanoparticles: Structures, synthesis, magnetic properties, surface functionalization, and emerging applications. *Applied Sciences, 11*(23), 11301. https://www.mdpi.com/2076-3417/11/23/11301

Olano, D. E. B., Salvador-Reyes, L. A., Montaño, M. N. E., & Azanza, R. V. (2020). Sorption of paralytic shellfish toxins (PSTs) in algal polysaccharide gels. *Algal Research, 45*, 101655. https://doi.org/10.1016/j.algal.2019.101655

Pillai, S. B. (2020). Adsorption in water and used water purification. In J. Lahnsteiner (Ed.), *Handbook of Water and Used Water Purification* (pp. 1–22). Springer. https://doi.org/10.1007/978-3-319-66382-1_4-1

Pini, R., Siderius, D. W., & Siepmann, J. I. (2022). Preface to adsorption and diffusion in porous materials special issue: Equilibrium adsorption data for energy and environmental applications. *Journal of Chemical & Engineering Data, 67*(7), 1597–1598. https://doi.org/10.1021/acs.jced.2c00382

Popa, S., Radulescu-Grad, M. E., Perdivara, A., & Mosoarca, G. (2021). Aspects regarding colour fastness and adsorption studies of a new azo-stilbene dye for acrylic resins. *Scientific Reports, 11*(1), 5889. https://doi.org/10.1038/s41598-021-85452-7

Pormazar, S. M., Ehrampoush, M. H., Ghaneian, M. T., Khoobi, M., Talebi, P., & Dalvand, A. (2020). Application of amine-functioned Fe_3O_4 nanoparticles with HPEI for effective humic acid removal from aqueous solution: Modeling and optimization. *Korean Journal of Chemical Engineering, 37*(1), 93–104. https://doi.org/10.1007/s11814-019-0411-y

Rápó, E., & Tonk, S. (2021). Factors affecting synthetic dye adsorption; desorption studies: A review of results from the last five years (2017–2021). *Molecules, 26*(17), 5419. https://www.mdpi.com/1420-3049/26/17/5419

Revellame, E. D., Fortela, D. L., Sharp, W., Hernandez, R., & Zappi, M. E. (2020). Adsorption kinetic modeling using pseudo-first order and pseudo-second order rate laws: A review. *Cleaner Engineering and Technology, 1*, 100032. https://doi.org/10.1016/j.clet.2020.100032

Santosa, S. J., Krisbiantoro, P. A., Yuniarti, M., Kustomo, & Koesnarpardi, S. (2021). Magnetically separable humic acid-functionalized magnetite for reductive adsorption of tetrachloroaurate(III) ion in aqueous solution. *Environmental Nanotechnology, Monitoring & Management, 15*, 100454. https://doi.org/10.1016/j.enmm.2021.100454

Sayed, N. S. M., Ahmed, A. S. A., Abdallah, M. H., & Gouda, G. A. (2024). ZnO@ activated carbon derived from wood sawdust as adsorbent for removal of methyl red and methyl orange from aqueous solutions. *Scientific Reports, 14*(1), 5384. https://doi.org/10.1038/s41598-024-55158-7

Shen, Z., Kuang, Y., Zhou, S., Zheng, J., & Ouyang, G. (2023). Preparation of magnetic adsorbent and its adsorption removal of pollutants: An overview. *TrAC Trends in Analytical Chemistry, 167*, 117241. https://doi.org/10.1016/j.trac.2023.117241

Shi, H., Ding, J., Timmons, T., & Adams, C. (2012). pH effects on the adsorption of saxitoxin by powdered activated carbon. *Harmful Algae, 19*, 61–67. https://doi.org/10.1016/j.hal.2012.05.008

Silva, R. A., Park, J., Lee, E., Park, J., Choi, S. Q., & Kim, H. (2015). Influence of bacterial adhesion on copper extraction from printed circuit boards. *Separation and Purification Technology, 143*, 169–176.

Svobodová, E., Tišler, Z., Peroutková, K., Strejcová, K., Abrham, J., Šimek, J., Gholami, Z., & Vakili, M. (2024). Adsorption of Cu(II) and Ni(II) from aqueous solutions using synthesized alkali-activated foamed zeolite adsorbent: Isotherm, kinetic, and regeneration study. *Molecules, 29*(10), 2357. https://www.mdpi.com/1420-3049/29/10/2357

Townhill, B. L., Tinker, J., Jones, M., Pitois, S., Creach, V., Simpson, S. D., ... & Pinnegar, J. K. (2018). Harmful algal blooms and climate change: Exploring future distribution changes. *ICES Journal of Marine Science, 75*(6), 1882–1893. https://doi.org/10.1093/icesjms/fsy113

Tran, H. N. (2023). Adsorption technology for water and wastewater treatments. *Water, 15*(15), 2857. https://www.mdpi.com/2073-4441/15/15/2857

Wang, T., Fernandes, S. P. S., Araújo, J., Li, X., Salonen, L. M., & Espiña, B. (2023). A carboxyl-functionalized covalent organic polymer for the efficient adsorption of saxitoxin. *Journal of Hazardous Materials, 452*, 131247. https://doi.org/10.1016/j.jhazmat.2023.131247

Zhang, Y., Whalen, J. K., Cai, C., Shan, K., & Zhou, H. (2023). Harmful cyanobacteria–diatom/dinoflagellate blooms and their cyanotoxins in freshwaters: A nonnegligible chronic health and ecological hazard. *Water Research, 233*, 119807. https://doi.org/10.1016/j.watres.2023.119807